JOURNAL OF GEOPHYSICAL RESEARCH, VOL. 102, NO. A7, PAGES 14,677–14,685, JULY 1, 1997

A two–dimensional simulation of the radial and latitudinal evolution of a solar wind disturbance driven by a fast, high–pressure coronal mass ejection

Pete Riley and J. T. Gosling

Los Alamos National Laboratory, Los Alamos, New Mexico

V. J. Pizzo

Space Environment Laboratory, National Oceanic and Atmospheric Administration, Boulder, Colorado

Abstract. Using a hydrodynamic simulation, we have studied the two–dimensional (symmetry in the azimuthal direction) evolution of a fast, high–pressure coronal mass ejection (CME) ejected into a solar wind with latitudinal variations similar to those observed by Ulysses. Specifically, the latitudinal structure of the ambient solar wind in the meridional plane is approximated by two zones: At low latitudes ($< 20°$) the solar wind is slow and dense, while at higher latitudes the solar wind is fast and tenuous. The CME is introduced into this ambient wind as a bell–shaped pressure pulse in time, spanning from the equator to 45° with a speed and temperature equal to that of the high–latitude solar wind. We find that such an ejection profile produces radically different disturbance profiles at low and high latitudes. In particular, the low–latitude portion of the ejecta material drives a highly asymmetric disturbance because of the relative difference in speed between the fast CME and slower ambient solar wind ahead. In contrast, the high–latitude portion of the same ejecta material drives a much more radially symmetric disturbance because the relative difference in pressure between the CME and ambient background plasma dominates the dynamics. The simulations reveal a number of other interesting features. First, there is significant distortion of the CME in the interplanetary medium. By ~ 1 AU the CME has effectively separated (in radius as well as latitude) into two pieces. The radial separation is due to the strong velocity shear between the slow and fast ambient solar wind. The latitudinal separation arises from pressure gradients associated with rarefaction regions that develop as the CME propagates outward. Second, there is significant poleward motion of the highest–latitude portion of the CME and its associated disturbance. The main body of the CME expands poleward by $\sim 18°$, while the forward and reverse waves (produced by the overexpanding portion of the CME) propagate all the way to the pole. Third, the simulations show that the high–pressure region, which develops at low latitudes as the fast CME ploughs through the slow ambient solar wind, penetrates significantly ($\sim 10°$) into the high–latitude fast solar wind. We compare the simulation results with a CME–driven interplanetary disturbance observed at both low and high latitudes and find that the simulation reproduces many of the essential features of the observations.

1. Introduction

The disruption of magnetically closed regions in the solar corona often leads to the eruption of large quantities of material from the solar atmosphere into interplanetary space. During these events, known as coronal mass ejections (CMEs), $10^{12} - 10^{13}$ Kg of material are typically released. CMEs play a central role in the large–scale evolution of the solar corona [e.g., *Hundhausen,* 1988] and are the prime cause of transient solar wind disturbances and large, non recurrent geomagnetic storms [e.g., *Gosling,* 1993].

At high heliographic latitudes, observations by the solar polar–orbiting spacecraft Ulysses have led to the identification of a new class of shock wave disturbances produced by CMEs [*Gosling et al.,* 1994]. Whereas in the ecliptic plane, transient shock wave disturbances

Paper number 97JA01131.
0148-0227/97/97JA-01131$09.00

are driven by a relative difference in speed between fast CMEs and slower ambient solar wind ahead, these high-latitude disturbances are driven by a relative difference in pressure between the CMEs and the surrounding ambient solar wind. It has been suggested that these "overexpanding" CMEs are ejected with internal pressures considerably larger than the surrounding solar wind but with comparable speeds [*Gosling et al.,* 1994]. The overpressure causes the CME to expand relative to the ambient solar wind, eventually producing an expansion front that surrounds it and a region of low pressure within the central portion of the CME. We note in passing that little distinction is made between strong compressive waves and shocks in this study. For simplicity, the term "shock" is used even when there may be some doubt that the wave has steepened sufficently to be labeled a shock.

One–dimensional (1–D) simulations have been quite successful in reproducing many of the essential features of observed CME–driven disturbances at low latitudes [*Hundhausen and Gentry,* 1969; *Hundhausen,* 1985] and high latitudes [*Gosling et al.,* 1994]. However, they cannot provide a self–consistent model of the global evolution of CME–driven disturbances and, furthermore, tend to overemphasize the strength of interactions through neglect of velocity shear. In this report we present results of a two–dimensional fluid simulation that mimics the ejection of a CME into interplanetary space and follows its subsequent evolution. We include sharp latitudinal variations in the ambient plasma flow based on Ulysses observations during its fast latitude scan in early 1995. Although the simulation is representative in the sense that we are not attempting to model any specific event in detail, we do compare our results with a CME–driven interplanetary disturbance that was observed by both Ulysses and IMP 8 at significantly different heliographic latitudes and heliocentric distances.

There have been a number of previous multidimensional fluid and MHD simulations of transient disturbances in the solar wind (see, for example, reviews by *Pizzo* [1985] and *Dryer* [1994]). Forward–reverse shock pairs are commonly produced in these simulations [e.g., *D'Uston et al.,* 1981; *Smith and Dryer,* 1990], as well as in one–dimensional fluid simulations [e.g., *Hundhausen and Gentry,* 1969], because of relative speed differences between fast initial perturbations to the flow and slower ambient wind ahead. On the other hand, shock pairs driven by relative speed differences are only rarely observed in CME–driven disturbances at low heliographic latitudes [e.g., *Gosling et al.,* 1988] and have yet to be observed in CME–driven disturbances at high latitudes. Several studies have considered disturbance propagation in a solar wind whose ambient properties vary with latitude. For example, *Krimsky and Transky* [1973] and *Odstrčil et al.* [1996] investigated shock wave propagation in a solar wind with simple latitudinal density variations. They found that the shock was impeded in regions of higher density.

The simulation presented in this paper differs from previous simulations in several important respects. First, as opposed to the simulations of *Gosling et al.* [1994, 1995], the simulation is two–dimensional. Second, the ambient solar wind in the present simulation includes, in addition to a large discontinuity in density, a large shear in flow speed that has not been considered explicitly in previous work. Third, the perturbing pulse at the inner boundary of the simulation, which mimics a CME, includes a combined velocity and density signal that leads to substantially different disturbance evolution at high and low latitudes. In particular, at high latitudes the disturbance is driven primarily by overexpansion of the mimicked CME, while at low latitudes the disturbance is driven primarily by the relative speed between the CME and the ambient wind. Fourth, in contrast to many previous two– and three–dimensional fluid and MHD simulations that simply introduce shock disturbances at an inner boundary, our simulation both includes and tracks the evolution of the perturbing CME.

Our simulation does not explicitly include the magnetic field. We are therefore obviously unable to address questions related to the magnetic structure of the CME, and the characteristic speed with which pressure disturbances propagate in the simulation is less than in the real solar wind. Further, magnetic forces, including those associated with pressure gradients and magnetic tension, are not included. Thus, although we find it convenient to mimic an initial high internal CME pressure with a density pulse, in real events the high internal pressure may also be a consequence of either high temperature or high magnetic field strength or both. Despite these limitations, gasdynamic calculations have proven to be extremely useful in the past in illuminating fundamental aspects of the processes by which both transient and corotating disturbances evolve in the solar wind (see, for example, reviews by *Hundhausen* [1985] and *Gosling* [1996]). They provide an excellent starting point for understanding how strong latitudinal shears in the ambient solar wind affect the evolution of solar wind disturbances associated with CMEs having high initial internal pressure and that span both high and low heliographic latitudes. We expect that simulations that include the magnetic field will obtain results in qualitative agreement with the present simulation although differing in some of the quantitative details.

2. Simulation of a CME-Driven Disturbance in a Two-Dimensional Solar Wind

The numerical model employed in this study is a single–fluid, two-dimensional, hydrodynamic code that uses Eulerian finite differencing [*Stone and Norman,* 1992]. Magnetic fields, radiation transport, and rotation are neglected. The internal energy is treated with the polytropic approximation and $\gamma = \frac{5}{3}$.

The simulations are performed in a meridional (north–south) plane with axisymmetry imposed in the azimuthal (east–west) direction. The modeling region extends in heliocentric distance from 30 solar radii ($R_\odot$) ($\sim$ 0.14 AU) to 5 AU and in latitude from the equator to the pole. Thus the entire modeling region is supersonic, and all disturbances (especially, reverse waves/shocks that propagate back toward the Sun in the rest frame of the solar wind) are convected away from the Sun. At the inner (radial) boundary, inflow boundary conditions are imposed. This is achieved by holding the flow fixed at predetermined values. Outflow boundary conditions are imposed at the outer boundary by setting the flow at the boundary equal to the flow just interior to it. This method for handling outflow is precise for supersonic flow [e.g., *Stone and Norman,* 1992] and thus appropriate for the present study. The mesh spacing is 2 $R_\odot$ in radius and 1° in latitude. Reflecting boundary conditions are imposed at the equator to ensure that the simulation is symmetric about the equator. Owing to the assumed symmetry in the azimuthal direction, any transient phenomena in the simulation must necessarily be toroidal in character.

The background solar wind flow structure is characterized by dense, slow radial flow from the equator to 20° and fast, tenuous radial flow from 20° to the pole. The two regions are separated by a thin transition layer (see below). At the inner boundary we specify the low– and high–latitude solar wind speed (v_o^l and v_o^h, respectively), high–latitude number density (n_o^h) and temperature (T_o^h), and the ratio of low– to high–latitude density (g). The temperature in the slow flow is adjusted so that the gas pressure at low latitudes is the same as in the fast flow along the inner radial boundary. Experience with 1–D simulations [e.g., *Gosling et al.,* 1994, 1995; *Gosling and Riley,* 1996] has provided us with a good indication of the types of densities, temperatures, and speeds at 30 $R_\odot$ that produce reasonable matches with Ulysses observations at larger heliocentric distances. For the specific simulation described here, we set $v_o^l = 250$ km s^{-1}, $v_o^h = 500$ km s^{-1}, $n_o^h = 500$ cm^{-3}, $T_o^h = 5 \times 10^6$ K, and $g = 3$. Note that mass and momentum fluxes in the two regions along the inner boundary differ. Ulysses observations have suggested that the mass flux may be as much as $\sim$ 47% higher near the equator than over the poles and momentum flux may be $\sim$ 20% higher over the poles than at near–equatorial latitudes [*Phillips et al.,* 1995; *Riley et al.,* 1997]. The values used here correspond to a 50% increase in the mass flux from pole to equator and a 25% increase in momentum flux from equator to pole. These values are used to fill the entire simulation region, and the program is run until a steady state equilibrium flow is reached.

Plate 1 shows radial and meridional (positive northward) velocity components and pressure after the equilibrium flow is achieved. The left panel emphasizes the sharp gradient in speed between the low– and high–latitude regions. Color contours of density and temperature are qualitatively similar to this. In the high–latitude solar wind, the plasma initially travelling at 500 km s^{-1} at the inner boundary is accelerated to $\sim$ 750 km s^{-1} over several tenths of an astronomical unit. At low latitudes the flow is accelerated from 250 km s^{-1}

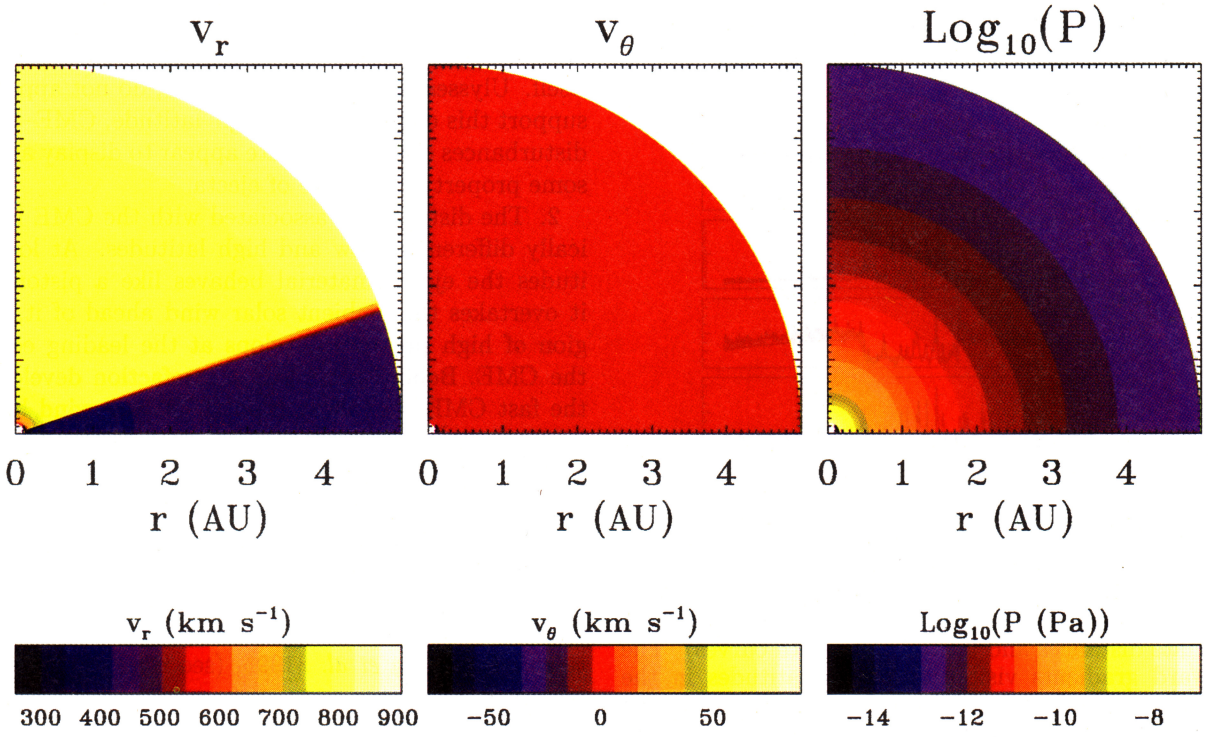

Plate 1. Color–coded plots of radial velocity, meridional (positive northward) velocity, and pressure for the steady state solution used in the simulation.

to $\sim$ 450 km s^{-1} over a comparable distance. Radial flow dominates the steady state solution, and the meridional flow in the middle panel is negligible everywhere. In the right panel, pressure is displayed logarithmically. The decrease in pressure in the outward direction is the result of the spherical, adiabatic expansion of the solar wind. Although the pressure appears to be continuous across the slow/fast interface at all heliocentric distances, this is an artifact of displaying 8 orders of magnitude variation. Since the flows at low and high latitudes differ both in speed and temperature at the inner boundary, their acceleration profiles differ slightly too. This causes the thermal pressure to vary with latitude in the vicinity of the slow/fast interface. This variation, however, never exceeds $\sim$ 4% at any heliocentric distance. In turn, these pressure variations are responsible for small ($<$ 0.9 km s^{-1}) equatorward meridional flows near the velocity discontinuity. Although the velocity shear is specified as an instantaneous change (i.e., over a single mesh zone) at the inner boundary by $\sim \frac{1}{2}$ AU, artificial viscosity (used to treat shocks) spreads the shear over three mesh zones.

Figure 1 compares Ulysses measurements taken during an interval of 10 months during the fast latitude scan with the steady state equilibrium reached by our model (smooth curves). During this interval, Ulysses moved from 80.2°S to 80.2°N, and from 2.3 AU to 1.34 AU (aphelion) and back out to 2.3 AU. This radial variation is responsible for the small poleward gradients in density, temperature, and thermal pressure at high latitudes. Our steady state simulation reproduces the essential large–scale features of the observations although it does not include stream structure or corotating interaction regions.

A perturbation is introduced into this ambient solar wind as a bell–shaped pressure pulse in time (in the form of an enhancement in density, $2 \times n_o^l$), centered on the equator, with a speed and temperature equal to that of the high–latitude solar wind. The pulse extends from the equator to 45° latitude and has a duration of 10 hours at the inner boundary. Thus, at low latitudes, the pulse is travelling significantly faster than the ambient solar wind, whereas at high latitudes it is coasting with the ambient solar wind. Also, at low latitudes the pulse is 2 times denser than the surrounding ambient solar wind, and at high latitudes it is 6 times denser than the ambient solar wind. However, since the pulse is also 3 times hotter than the surrounding solar wind at low latitudes, the initial peak pressure of the pulse is a factor of 6 higher than the surrounding solar wind in both the low– and high–latitude regions. Thus the pulse mimics the ejection of a fast CME that initially has a higher internal pressure than the ambient wind at both high and low latitudes. Tracer particles (180 in all) are added around the boundary of the ejected CME (60 each on the front side, back side, and top). These allow us to track the boundary of the ejecta material, which would otherwise be difficult, if not impossible, to infer based solely on the overall disturbance profiles.

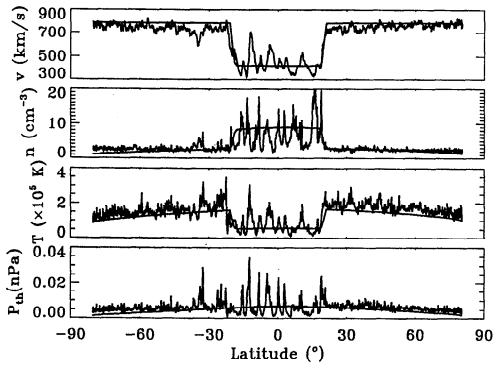

Figure 1. Ulysses measurements of proton speed, number density, temperature, and thermal pressure during the fast latitude scan in early 1995 compared with the steady state equilibrium solution at the appropriate distances and latitudes (smooth curves). The poleward gradients visible at higher latitudes in the lower three panels reflect Ulysses' radial motion during this interval, moving from 2.3 AU to 1.34 AU (aphelion) and back out to 2.3 AU.

Plate 2 shows snapshots of radial velocity, meridional velocity, and pressure taken at 167 hours (6.9 days) after the ejection of the CME. The boundary of the CME is marked with the solid line. We note the following:

1. At launch the maximum latitudinal extent of the CME is 45°. By 167 hours, the CME extends poleward to $\sim$ 63°, and its associated forward and reverse waves have reached the pole. Most of this poleward expansion occurs close to the Sun where, because of the diverging geometry, latitudinal distances are relatively small. This suggests that it might be fairly common to observe disturbances associated with CMEs at higher latitudes without ever encountering the ejecta material itself. Ulysses observations, however, do not appear to support this conjecture: all high–latitude, CME–driven disturbances observed to date appear to display at least some property indicative of ejecta.

2. The disturbance associated with the CME is radically different at low and high latitudes. At low latitudes the ejecta material behaves like a piston. As it overtakes the ambient solar wind ahead of it, a region of high pressure develops at the leading edge of the CME. Behind the CME a rarefaction develops as the fast CME runs away from the slower wind behind it. This result is qualitatively similar to the 1–D simulations by *Gosling et al.* [1995] (see their Figure 3, bottom panel). At higher latitudes the disturbance associated with the CME is much more symmetric with radius about the CME. The initial overpressure within the CME drives a pair of relatively weak shocks. This result is also qualitatively similar to the 1–D simulations by *Gosling et al.* [1995] (see their Figure 3, top panel).

3. By $\sim$ 1 AU the CME has essentially separated into two pieces. The radial separation is caused by the

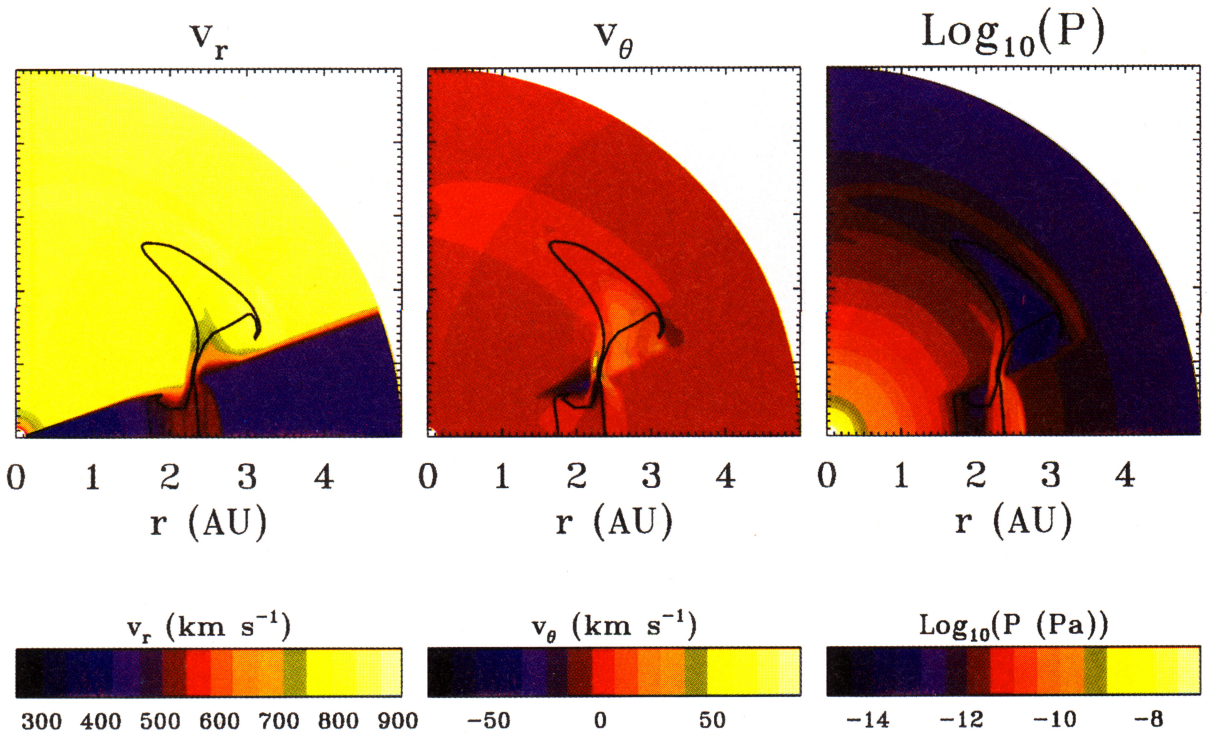

Plate 2. Color–coded plots of radial velocity, meridional velocity, and pressure ~ 7 days after the launch of a coronal mass ejection. The CME is introduced into the ambient solar wind as a bell–shaped pressure pulse (in the form of a density enhancement) over an interval of 10 hours, with a speed and temperature equal to that of the high–latitude solar wind. The solid line marks the boundary of the CME.

strong velocity shear between the slow and fast ambient solar wind. The CME also separates in latitude because of the rarefaction regions which develop in each of the two portions of the CME. At high latitudes the expansion of the high–pressure CME causes a rarefaction region to develop within the CME which drives poleward motions of the plasma. At low latitudes the fast CME outruns the slower plasma behind it, and a rarefaction (expansion) wave propagates both back into the slow solar wind behind the CME and forward into the CME itself. This rarefaction region drives an equatorward flow of plasma. The net result is that high–speed ambient plasma is sucked to lower latitudes just poleward of the low–latitude portion of the CME, and slower ambient wind located just equatorward of the high–lattude portion of the CME is sucked to higher latitudes. Toward the leading and trailing edges of both portions of the CME, where the rarefactions disappear, the meridional flow away from the slow/fast interface ceases, and the sheared boundaries of both the low– and high–latitude portions of the CME develop a bowed shape.

4. Thoughout the CME and its associated disturbance there is significant meridional flow. Within the CME the large–scale meridional flow is poleward at latitudes greater than the slow/fast solar wind interface ($\gtrsim 20°$). Below 45° the plasma flow is primarily driven by the formation of a rarefaction region as discussed above. At higher latitudes the plasma flow is a remnant of the poleward motion caused by the strong pressure gradient between the initially dense CME and the tenuous high–latitude ambient plasma. In the sheath region between the forward and reverse shocks and the CME at latitudes $\gtrsim 20°$, the meridonal component of the flow is also poleward. This flow can be explained in the following way: The shock fronts lie on elliptical lines, with the radial distance to the shock being less at higher latitudes, a consequence of the finite travel time of the disturbance waves toward the pole. For gasdynamic shocks (as well as fast mode shocks), plasma is deflected away from the shock normal as it flows across the shock front. Since the upstream flow is radial, the plasma must be deflected poleward for both the forward and the reverse shock. Similar arguments can be applied to the flow across the forward shock at low latitudes. This relies on the assumption that the CME is launched at all latitudes at the same time. For more complex geometries the flow deflections might be different.

Since there is considerable latitudinal and radial variation in the ambient solar wind flow, it is worthwhile considering the relative perturbations. Plate 3 shows difference images of v_r, v_θ, and $\log(P)$, relative to the equilibrium–flow solution. Thus the slow/fast speed discontinuity and radial variation in pressure have been removed, and the perturbations driven by the CME are emphasized.

We focus first on the low–latitude portion of the CME disturbance, where initally two pairs of waves are gener-

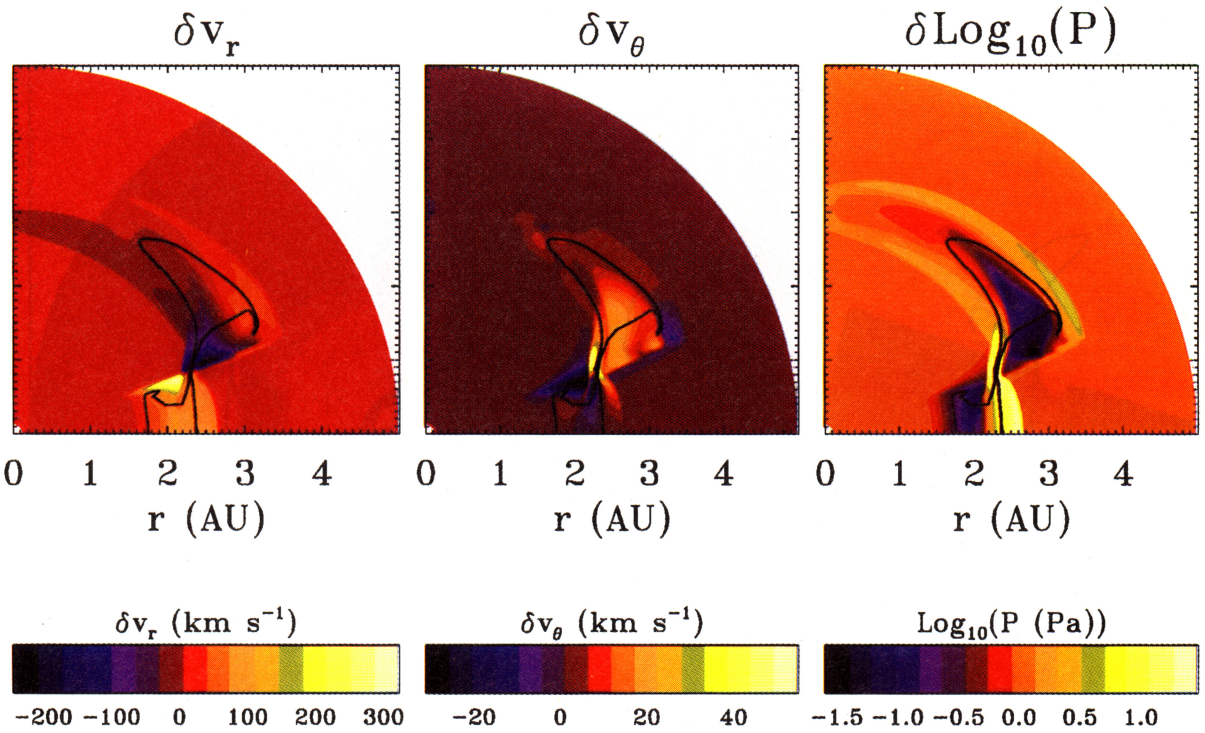

Plate 3. Same as Plate 2, except that the difference between the solution at ~ 7 days and the initial steady state solution is shown.

ated. Since the CME is overtaking and compressing the ambient wind ahead, a region of high pressure develops which is bounded by forward and reverse waves/shocks. Furthermore, the CME is denser than the surrounding plasma; as it expands, a pair of forward and reverse waves form centered on the CME and propagating away from it. The evolution of this system has been discussed by *Gosling et al.* [1995]. Briefly, the reverse wave associated with the expansion of the compressed region at the leading edge of the CME interacts with the forward wave associated with the expansion of the CME, weakening both in the process. Furthermore, since the CME is propagating away from the slow ambient solar wind behind it faster than the reverse wave associated with the expansion of the CME can propagate, the reverse shock associated with the expansion of the CME does not develop. It is interesting that the high–pressure region at the front of the disturbance is not confined by the original slow/fast latitude interface. On the contrary, it extends poleward by ~ 10° into the fast solar wind. This poleward expansion is associated with the strongest meridional velocities (~ 50 km s^{-1}) within the disturbance.

At high latitudes the center of the CME is traveling out from the Sun at the same speed as the ambient solar wind. The forward and reverse waves are created by the expansion of the high–pressure CME into the surrounding solar wind, and the evolution proceeds in a much more symmetric fashion. The pressure at the leading edge of the disturbance maximizes at latitudes < 45°, which maps to the initial latitudinal extent of the CME.

3. Comparison With Observations

The simulation discussed in the present study is representative in the sense that we have not attempted to model any specific observed CME–driven disturbance. Nevertheless, it is instructive to make a qualitative comparison of our results with a disturbance that was observed at two significantly different latitudes and distances in the heliosphere. *Gosling et al.* [1995] presented high– and low–latitude measurements of a CME–driven solar wind disturbance observed by Los Alamos plasma instruments onboard IMP 8 and Ulysses in late February to early March 1994. At the time, Ulysses was located at a heliocentric distance of 3.53 AU and 54°S. IMP 8 was 7° below the heliographic equator at a distance of 1 AU, and the two spacecraft were separated by ~ 18° in solar longitude.

Figure 2 compares Ulysses observations of this event with our simulation results. Note that the y axis scales are not the same; they have been constructed so as to emphasize variations in the parameters. Figure 2a shows Ulysses measurements of proton speed, density, and temperature for a period of 6 days in late February to early March 1994. The CME interval, as identified by counterstreaming suprathermal electrons [*Gosling et al.*, 1995], is indicated by the two dotted vertical lines, and the forward and reverse shocks propagating away from the CME are marked with the solid vertical lines labeled F and R. Several interesting features are apparent. First, the CME–disturbance profile is fairly symmetric (as a function of time). The forward and reverse shocks bounding the CME are positioned at ap-

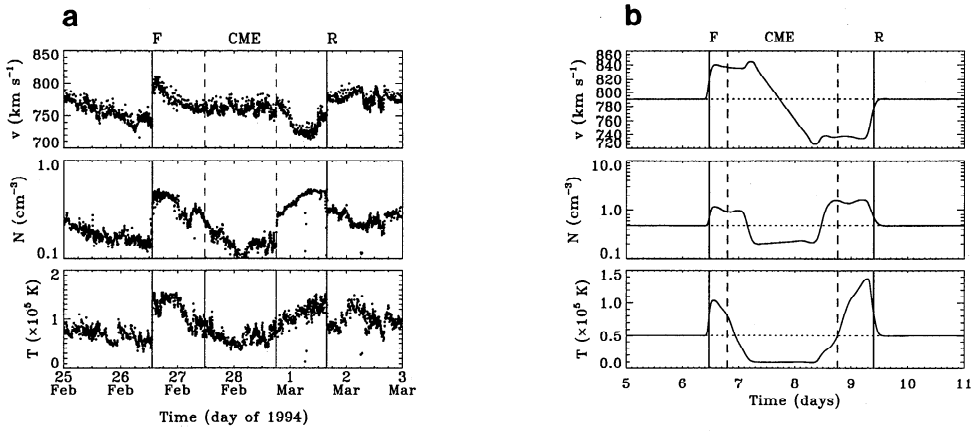

Figure 2. (a) Proton speed (v), number density (N), and temperature (T) profiles for a CME observed by Ulysses at 3.53 AU and 54°S [after *Gosling et al.*, 1995]. (b) Simulation results at the same heliocentric distance as Ulysses but at 35° latitude. Time in the simulation refers to the time since the launch of the CME pulse.

proximately the same time interval before and after the CME. Second, the speeds before the disturbance, during the CME interval, and after the disturbance are all approximately the same. Third, there is a slight asymmetry in the shocks; the forward shock exibits a larger jump in speed, density, and temperature, indicating that it is the stronger of the two. Figure 2b shows our simulation results at 3.53 AU and $\sim 35°$. In reality, Ulysses observed the CME at $\sim 54°$. However, in order to reduce the potential contamination of our simulation results with waves reflecting at the poles (which result from the ejection of a torus), we restricted the initial latitudinal extent of the CME to 45°. Thus we make our comparison at $\sim 35°$. The time indicated along the x axis is measured relative to the launch of the CME from the inner boundary at 30 $R_\odot$.

Comparison between Figures 2a and b demonstrates that our simulation has reproduced many of the essential features of the Ulysses observations. Both the forward and reverse shocks stand off from the CME at roughly comparable times (although this time is significantly less in the simulations). The least favorable aspect of the comparison concerns the speed profile within the CME; our simulation indicates that the CME is still undergoing some expansion (the leading edge of the CME is travelling $\sim$ 80 km s^{-1} faster than the trailing edge of the CME), whereas the CME observed by Ulysses shows essentially no further expansion. It should, however, be emphasized that all of the remaining overexpanding CMEs observed by Ulysses show declining speed profiles across the CME, similar to the simulation.

Figure 3 compares low–latitude (7°) observations by IMP 8 with our simulation. Again note that the y axis scales are not identical. IMP 8 observed a far more asymmetric disturbance than Ulysses. The disturbance did not include a reverse shock, and the CME was moving at speeds in excess of 250 km s^{-1} relative to the ambient solar wind ahead. The CME was identified by low proton temperature, high He abundance, and a strong but declining magnetic field strength of low variance which rotated $\sim 120°$ in azimuth [*Gosling et al.*, 1995].

Comparison of Figures 3a and b demonstrates the reasonably good agreement between simulation and ob-

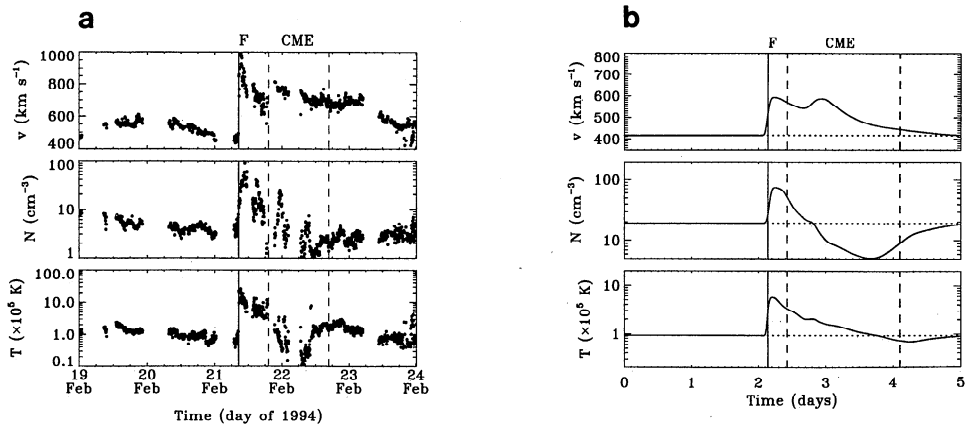

Figure 3. Same parameters as Figure 2 but for IMP 8 at low latitudes [after *Gosling et al.*, 1995]. (b) Simulation results at same latitude and heliocentric distance as IMP 8.

servations at low latitudes. There is at least one significant difference, however, concerning the extent of the CME. In our simulations the CME takes $\sim$ 1.75 days to pass 1 AU. Observationally, however, the CME is inferred to be $\sim$ 1 day in duration. In addition, the observed forward shock stands off at a slightly larger distance than our simulation suggests.

We have identified four possible reasons that may explain the disagreements between the model and the observations. First, the CME probably had a far more complicated geometry at launch than was mimicked by our simulation. We suspect that the CME was not ejected at the same speed at all latitudes. In fact, the IMP 8 observations strongly suggest that the CME initially was traveling significantly faster at near–equatorial latitudes than at high latitudes. Second, the solar wind expansion is not strictly adiabatic as is assumed in the simulation. Thus we cannot adjust our inner boundary ambient plasma values so that they simultaneously provide a good match at both 1 and 3.5 AU. This problem could be partially cimcumvented by reducing the polytropic index [*Totten et al.*, 1996]. Third, in reality, the geometry of the slow–fast transition occurs on a tilted spiral front which changes with heliocentric distance. Thus our neglect of variations in the azimuthal direction does not allow for any east–west interactions, stream structure, or limited azimuthal extent of the CME. Fourth, we neglect the magnetic field. One consequence of this is that waves in the simulation travel at the sound speed, which can be considerably less than the magnetosonic speed. The smaller shock standoff times in the simulation results can probably be attributed to this.

4. Summary and Discussion

Using a two–dimensional fluid model, we have simulated the ejection of a fast, high–pressure CME into a solar wind containing latitudinal gradients similar to those observed during Ulysses' fast latitude scan. Comparison of these results with a CME–driven disturbance observed both by Ulysses at high latitudes and IMP 8 at low latitudes indicate that we have reproduced many of the essential features of the observations.

In spite of the simplifying assumptions used in the simulation, the results display considerable complexity. An outstanding feature is the way in which the CME separates into two pieces, both in latitude and heliocentric distance. The strong velocity shear at 20° is responsible for the separation in distance. The separation in latitude is due to rarefaction regions that develop as the CME propagates away from the Sun; the sheared CME boundary on either side of the slow/fast speed interface is effectively sucked away from the interface. There is also considerable poleward expansion of the highest latitude portion of the CME and its associated disturbance. The CME expands poleward by $\sim$ 18°, and the forward and reverse waves propagate all the way to the pole. In addition, the high-pressure region, which develops at the leading edge of the CME at low–latitudes as it ploughs through the slow ambient solar wind, penetrates significantly ($\sim$ 10°) into the high–latitude solar wind.

The rich complexity of the simulation results indicate that a single CME can present radically different profiles in interplanetary space depending on the latitude at which it is observed. We have highlighted two such profiles in this study for comparison with Ulysses and IMP 8 observations. Let us now consider what a spacecraft located at several astronomical units and $\sim$ 22° latitude would observe for the event simulated. From Plate 3 we would infer that there would be little or no signatures of ejecta. On the other hand, the spacecraft might see a weak forward shock (due to the expansion of the high–latitude portion of the CME) followed by a rarefaction region, a second strong forward shock, and a strong reverse shock (from the penetrating portion of the low–latitude high–pressure region) bounding any remains of the CME. Since this complicated profile is driven to a large degree by meridional fluid motions, this is not a result that could be obtained from a 1–D simulation. By extension, these results suggest that three–dimensional calculations including stream structure and interaction regions will likely produce an even richer set of results.

The latitudinal gradients in the ambient solar wind speed, density, and temperature clearly have a strong effect on the large–scale evolution of the CME and its associated disturbance. Our simulation results suggest that the global shape of the CME is convex except in the vicinity of the slow/fast interface. This is simply a result of the near constancy of the ambient solar wind speed within each region. This geometry may be contrasted with previous visualizations of mid– and high–latitude CMEs. First, *Hammond et al.* [1995] proposed a concave shape (in the meridional plane) for a CME-driven disturbance observed by both Geotail and Ulysses in December–January 1993 at significantly different latitudes and heliocentric distances (see their Figure 5). This inferrence was based on the arrival times of the disturbances at the two spacecraft and the speeds of the CMEs. An alternative interpretation, based on the results of the present study and consistent with the observations, is that there existed a strong velocity shear between the two spacecraft. We suggest the global shape of the CME may have been convex, except in the vicinity of the velocity discontinuity. Second, *Gosling et al.* [1994] proposed that some high—latitude, CME–driven disturbances might be elliptical in shape with an expansion shock or wave that wrapped completely around the CME. This picture, however, implies that the CME is launched exclusively into fast solar wind. Although our simulation results differ from this picture of an elliptically shaped disturbance, they do provide a mechanism by which isolated ejecta may be produced in the fast solar wind as envisaged by *Gosling et al.*

[1994]. In reality, the geometry of the CME is likely to be more complicated than either an ellipsoid or the shape calculated in the idealized simulation presented here.

Acknowledgments. The work at Los Alamos was performed under the auspices of the U.S. Department of Energy and was supported by a laboratory–directed research and development grant. The work by V.J.P. at NOAA/SEC was supported in part by NASA grants.

The editor thanks two referees for their assistance in evaluating this paper.

References

Dryer, M., Interplanetary studies: Propagation of disturbances between the Sun and the magnetosphere, *Space Sci. Rev., 67,* 363, 1994.

D'Uston, C., M. Dryer, S. M. Han, and S. T. Wu, Spatial structure of flare–associated perturbations in the solar–wind simulated by a two–dimensional numerical MHD model, *J. Geophys. Res., 86,* 525, 1981.

Gosling, J. T., The solar flare myth, *J. Geophys. Res., 98,* 18,937, 1993.

Gosling, J. T., Corotating and transient solar wind flows in three dimensions, *Annu. Rev. Astron. Astrophys., 34,* 35, 1996.

Gosling, J. T., and P. Riley, The acceleration of slow coronal mass ejections in the high speed solar wind, *Geophys. Res. Lett., 23,* 2867, 1996.

Gosling, J. T., S. J. Bame, E. J. Smith, and M. E. Burton, Forward–reverse shock pairs associated with transient disturbances in the solar wind at 1 AU, *J. Geophys. Res., 93,* 8741, 1988.

Gosling, J. T., D. J. McComas, J. L. Phillips, L. A. Weiss, V. J. Pizzo, B. E. Goldstein, and R. J. Forsyth, A new class of forward-reverse shock pairs in the solar wind, *Geophys. Res. Lett., 21,* 2271, 1994.

Gosling, J. T., D. J. McComas, J. L. Phillips, V. J. Pizzo, B. E. Goldstein, R. J. Forsyth, and R. P. Lepping, A CME-driven solar wind disturbance observed at both low and high heliographic latitudes, *Geophys. Res. Lett., 22,* 1753, 1995.

Hammond, C. M., G. K. Crawford, J. T. Gosling, H. Kojima, J. L. Phillips, H. Matsumoto, A. Balogh, L. A. Frank, S. Kokubun, and T. Yamamoto, Latitudinal structure of a coronal mass ejection inferred from Ulysses and Geotail observations, *Geophys. Res. Lett., 22,* 1169, 1995.

Hundhausen, A. J., Some macroscopic properties of shock waves in the Heliosphere, in *Collisionless Shocks in the Heliosphere: A Tutorial Review, Geophys. Monogr. Ser.,* vol. 34, edited by R. G. Stone and B. T. Tsurutani, pp. 37–58, AGU, Washington, D.C., 1985.

Hundhausen, A. J., The origin and propagation of coronal mass ejections, in *Proceedings of the Sixth International Solar Wind Conference,* edited by V. J. Pizzo, T. E. Holzer, and D. G. Sime, *Tech. Note TN-306,* pp. 181–214, Natl. Cent. for Atmos. Res., Boulder, Colo., 1988.

Hundhausen, A. J., and R. A. Gentry, Numerical simulation of flare–generated disturbances in the solar wind, *J. Geophys. Res., 74,* 2908, 1969.

Krimsky, G. F. and I. A. Transky, Shock–wave propagation in the interplanetary medium, II, *Geomagn. and Aeron., 13,* 660, 1973.

Odstrčil, D., M. Dryer, and Z. Smith, Interaction of an interplanetary shock with the heliospheric plasma sheet, *Solar Wind Eight: Proceedings of the Eighth International Solar Wind Conference,* edited by D. Winterhalter, J. T. Gosling, S. R. Habbal, W. S. Kurth, and M. Neugebauer, *AIP conf. Proc. 382,* 457, 1996.

Phillips, J. L., et al., Ulysses plasma observations from pole to pole, *Geophys. Res. Lett., 22,* 3301, 1995.

Pizzo, V. J., Interplanetary shocks on the large scale: A retrospective on the last decades theoretical efforts, in *Collisionless Shocks in the Heliosphere: Reviews of Current Research, Geophys. Monogr. Ser.,* vol. 35, edited by B. T. Tsurutani and R. G. Stone, pp. 51–68, AGU, Washington, D.C., 1985.

Riley, P., S. J. Bame, B. L. Barraclough, W. C. Feldman, J. T. Gosling, G. W. Hoogeveen, D. J. McComas, J. L. Phillips, B. E. Goldstein, and M. Neugebauer, Ulysses solar wind plasma observations at high latitudes, *Advances in Space Res.,* in press, 1997.

Smith, Z., and M. Dryer, MHD study of temporal and spatial evolution of simulated interplanetary shocks in the ecliptic–plane within 1 AU, *Solar Phys., 129,* 387, 1990.

Stone, J.M., and M. L. Norman, ZEUS-2D: A radiation magnetohydrodynamics code for astrophysical flows in two space dimensions. I. The hydrodynamic algorithms and tests, *Astrophys. J., 80,* 753 , 1992.

Totten, T. L., J. W. Freeman, and S. Arya, Application of the empirically derived polytropic index for the solar–wind to models of solar–wind propagation, *J. Geophys. Res., 101,* 15,629, 1996.

J. T. Gosling and P. Riley, Space and Atmospheric Sciences Group, NIS-1, MS D466, Los Alamos National Laboratory, Los Alamos, NM 87545. (e-mail: jgosling@lanl.gov; uk2@lanl.gov)

V. J. Pizzo, Space Environment Laboratory, National Oceanic and Atmospheric Administration, Mail Code R/E/SE, 325 South Broadway, Boulder, CO 80303. (e-mail: vpizzo@sec.noaa.gov)

(Received January 31, 1997; revised April 11, 1997; accepted April 14, 1997.)